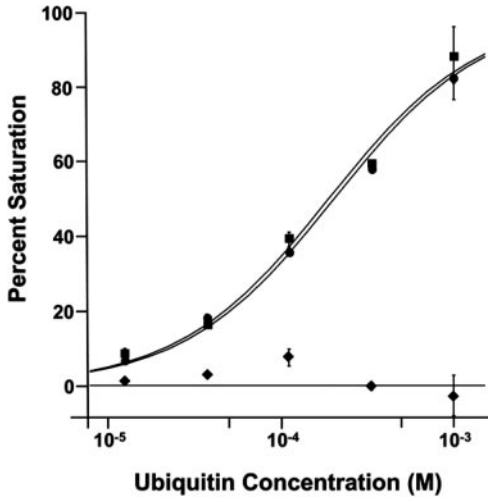

FIG. 5. Biosensor binding analyses of $EAP45_{1–229}$-ubiquitin interactions. Binding isotherms for wild-type Ub (circles) (K_D = 210 ± 10 μM), F4A Ub (squares) (K_D = 170 ± 10 μM), and I44A Ub (diamonds) (K_D > 1 mM) binding to immobilized GST-$EAP45_{1–229}$. The error bars represent standard deviations.

lack NZF motifs, however, and it has therefore been unclear whether they could still interact with ubiquitylated protein cargoes. This puzzle has recently been resolved by Slagsvold and colleagues, who showed that a minimal N-terminal fragment of murine EAP45 spanning residues 1 to 139 binds directly to ubiquitin (K_D = 460 μM) and also binds phosphoinositides (67).

We independently tested for ubiquitin binding activity in the human EAP45 protein using the entire region of human EAP45 that is missing from the crystal structure of yeast Vps36p ($EAP45_{1–229}$). Biosensor binding analyses revealed that ubiquitin bound specifically to GST-$EAP45_{1–229}$, with an estimated dissociation constant of 210 ± 10 μM in the experiment shown in Fig. 5. $EAP45_{1–229}$ binding was strongly inhibited by the Ub I44A mutation, but not by a F4A mutation, demonstrating that the exposed hydrophobic Ub I44 surface forms at least part of the EAP45 binding site. This same binding surface is also recognized by nearly all of the other ubiquitin binding proteins characterized to date (29). Ubiquitin also bound with a similar affinity to a minimal $EAP45_{1–139}$ construct (K_D = 410 ± 90 μM; n = 6), indicating that the ubiquitin binding site is located within the N-terminal GLUE domain. These data are all in excellent agreement with recent analyses of ubiquitin binding to the murine EAP45 GLUE domain (67).

EAP20 and CHMP6 accumulate on aberrant endosomal class E compartments in the absence of VPS4 ATPase activity. Under steady-state conditions, all three ESCRT complexes are predominantly cytoplasmic but assemble transiently on the endosomal membrane to participate in vesicle formation. The assembled ESCRT complexes are then recycled off the endosomal membrane by the action of the VPS4 AAA ATPases (5). Inhibition of human and yeast VPS4 ATPase activity therefore traps class E proteins, including the VPS4 proteins themselves, on aberrant endosomal class E compartments (3–5, 8, 21, 83, 89).

To test whether human ESCRT-II associated with endosomal membranes in a VPS4-dependent fashion, we examined the localization of two different ESCRT-II components, EAP20 and EAP30, in the presence of a mutant VPS4A protein (green fluorescent protein [GFP]-$VPS4A_{K173Q}$) previously shown to block ATP binding and to dominantly inhibit VPS4 activity in cells (8). As shown in Fig. 6A and B, antibodies against EAP20 detected endogenous EAP20 in COS-7 cells, albeit weakly. These antibodies also cross-reacted with a second protein of ~36 kDa (data not shown). We therefore also examined the localization of exogenous, Myc-tagged EAP20 to take advantage of the enhanced immunofluorescence signal of the tagged, overexpressed protein (Fig. 6C). In both cases, EAP20 localized to the enlarged endosomes induced by GFP-$VPS4A_{K173Q}$ overexpression. In the absence of GFP-$VPS4A_{K173Q}$, both endogenous and overexpressed EAP20 were distributed throughout the cytoplasm, as has been seen for other ESCRT complexes (Fig. 6B and D). To confirm that these results accurately represented the distribution of the entire ESCRT-II complex, the localization of a second ESCRT-II component, EAP30, was also examined. Once again, the overexpressed, Myc-tagged EAP30 protein was seen throughout the cell, but it became trapped on the class E compartments induced by dominant-negative GFP-$VPS4A_{K173Q}$ (compare Fig. 6E and F). Hence, ESCRT-II was recruited to class E compartments, where it became trapped in the absence of VPS4 ATPase activity. Localization of the endogenous ESCRT-III protein, CHMP6, was also examined, and this protein was also strongly recruited to aberrant class E compartments (Fig. 6G and H and data not shown). Similar results were obtained using the other dominant-negative ATPase constructs, GFP-$VPS4A_{E228Q}$, DsRed-$VPS4B_{K180Q}$, and DsRed-$VPS4B_{E235Q}$ (22, 83), and with human osteosarcoma cells (data not shown). These data are all consistent with the idea that human EAP20/ESCRT-II, EAP30/ESCRT-II, and CHMP6/ESCRT-III function in vesicle formation and cargo sorting at the MVB.

HIV-1 particles are released efficiently from cells depleted of EAP20. To test whether ESCRT-II is required for efficient HIV-1 budding, we measured the levels of HIV-1 vector and virus production following siRNA depletion of EAP20 or TSG101 (positive control). As shown in Fig. 7A and C, both EAP20 and TSG101 were successfully depleted to nearly undetectable levels, as determined by quantification of Western blots of cellular extracts (Fig. 7A and C, "Cells," top two rows). Importantly, intracellular Gag expression levels were not significantly altered by depletion of either protein ("Cells," bottom rows). As expected, the release of virions was dramatically reduced upon TSG101 depletion (Fig. 7A and C, "Virions," lanes "TSG101"), and the infectious titers were reduced ~20-fold (Fig. 7B and D). Surprisingly, however, depletion of EAP20 did not significantly affect viral release as measured in Western blot assays (Fig. 7A and C, "Virions", lanes "EAP20"), and actually increased vector titers slightly at the 24-h time point (Fig. 7B and D, bars 4), although at a later time point (48 h), HIV-1 titers were reduced twofold (data not shown). We therefore conclude that efficient depletion of EAP20 does not significantly inhibit the release or infectivity of HIV-1.

HIV-1 particles are also efficiently released from cells depleted of CHMP6. The efficient release of HIV-1 from EAP20-